Update on EUV radiometry at PTB

Christian Laubis, Annett Barboutis, Christian Buchholz, Andreas Fischer, Anton Haase, Florian Knorr, Heiko Mentzel, Jana Puls, Anja Schönstedt, Michael Sintschuk, Victor Soltwisch, Christian Stadelhoff and Frank Scholze
Physikalisch-Technische Bundesanstalt, Abbestraße 2-12, 10587 Berlin, Germany (PTB)

ABSTRACT

The development of technology infrastructure for EUV Lithography (EUVL) still requires higher levels of technology readiness in many fields. A large number of new materials will need to be introduced. For example, development of EUV compatible pellicles to adopt an approved method from optical lithography for EUVL needs completely new thin membranes which have not been available before. To support these developments, PTB with its decades of experience [1] in EUV metrology [2] provides a wide range of actinic and non actinic measurements at in-band EUV wavelengths as well as out of band. Two dedicated, complimentary EUV beamlines [3] are available for radiometric [4,5] characterizations benefiting from small divergence or from adjustable spot size respectively. The wavelength range covered reaches from below 1 nm to 45 nm [6] for the EUV beamlines [5] to longer wavelengths if in addition the VUV beamline is employed. The standard spot size is 1 mm by 1 mm with an option to go as low as 0.1 mm to 0.1 mm. A separate beamline offers an exposure setup. Exposure power levels of 20 W/cm^2 have been employed in the past, lower fluencies are available by attenuation or out of focus exposure. Owing to a differential pumping stage, the sample can be held under defined gas conditions during exposure. We present an updated overview on our instrumentation and analysis capabilities for EUV metrology and provide data for illustration.

Keywords: EUV, at-wavelength, radiometry, metrology, reflectometry, exposure

1. INTRODUCTION

A large number of new materials will need to be introduced for the further development of EUV lithography as for the production of new semiconductor devices in general. All those materials need to be characterized for their optical properties with respect to their behavior in lithography for optical measurements in process control. Material for the EUV optical systems must also be validated for their endurance under EUV exposure [7]. PTB has established a suite of instrumentation and experience to measure the data required to answer these questions. With further developments in mind, we work on cleaner sample environments, better lateral measurement resolution and lifetime/exposure tests.

2. INSTRUMENTATION

PTB operates two beamlines for measurements in the EUV spectral region [3]. The EUV beamline [8] at the MLS [9] (5.5 nm to 48 nm) with the large reflectometer [10] for samples up to collector size with adjustable spot size from 0.1 mm x 0.1 mm to 4 mm x 4 mm is complemented by the soft X-ray beamline (from below 1 nm to 25 nm) at BESSY II, optimized for low beam divergence to facilitate scatter measurements [11] and equipped with an un-lubricated instrument for measurements with arbitrarily rotated plane of reflection.

2.1 New experimental stage at second focus for the EUV beamline

At the EUV beamline, we installed an additional toroidal mirror behind the existing instrumentation to image the first focus at the center of the large reflectometer into a second focus at an additional measurement station. This second focus is most useful for the characterization of small detectors [12,13] and a dedicated measurement station for detectors has been set up. Figure 1 shows the beamline setup from source point (far left) via 1st focus (at position 'reflectometer'), to 2nd focus on the far right.

Extreme Ultraviolet (EUV) Lithography VII, edited by Eric M. Panning, Proc. of SPIE Vol. 9776, 977627 · © 2015 SPIE · CCC code: 0277-786X/15/$18 · doi: 10.1117/12.2218902

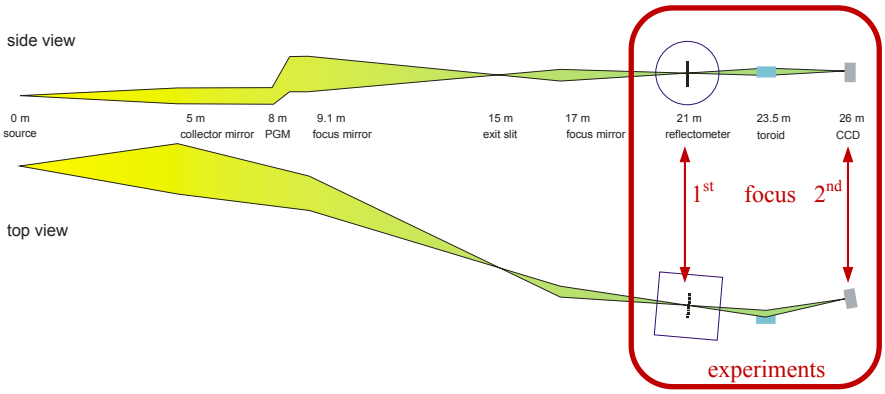

Figure 1:
EUV beamline from source point (left side) to experiment (right side). The first focus is located in the center of the reflectometer, the second focus is on the far right at the measurement station 'CCD'.

The refocusing into a second focus allows a spatial cleaning of the beam. Figure 2 shows 4 pictures of the beam at 2nd focus. Rows differ by scaling with the top row in linear intensity scale and the bottom row in logarithmic intensity scale. Columns differ by spatial filtering with the left column without extra filtering and the right column with spatial filtering by a horizontal aperture at 1st focus in the center of the reflectometer. As can be seen in Figure 2d, the spatial filtering reduces the beam halo significantly, thereby improving our ability to measure e.g. small detectors.

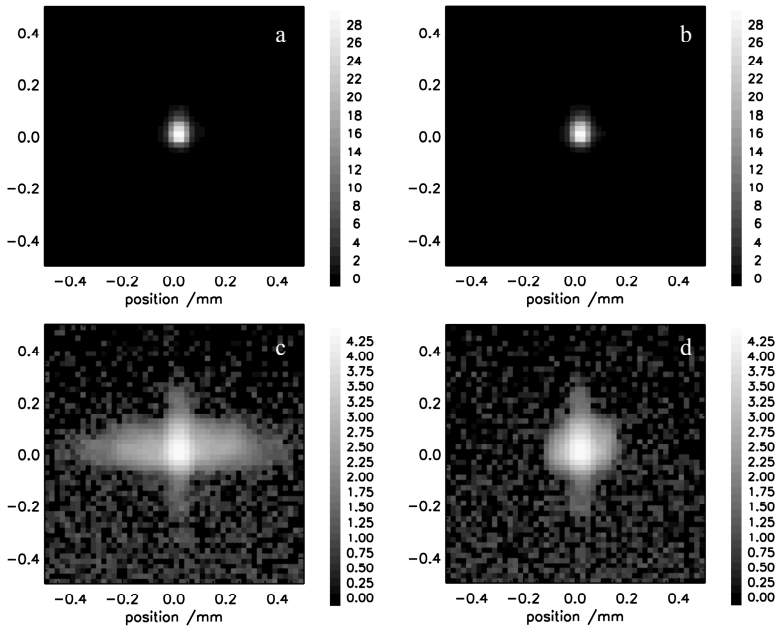

Figure 2:
Beam shape at 2nd focus.
For all pictures, beam size is 0.1 x 0.1 mm^2

Top row (a,b): Linear intensity scale.
The count numbers on the scale bar are divided by 10^3 for readability.

Bottom row (c,d): Logarithmic intensity scale.
The counts scale bar is in $\log_{10}$

Left column (a,c): No aperture at 1st focus

Right column (b,d): Additional spatial filtering by a horizontal aperture at 1st focus.

Low beam halo at 2nd focus is achieved by additional spatial filtering.

At the same time, refocusing the first focus of the beamline into a 2nd focus makes an additional measurement method available: Illuminating transmissive samples in the first focus and using a CCD as detector in the second focus provides fine-grained 2D transmission pictures. The beam illuminating the sample can be made as wide as 4 x 4 mm^2. As an example for this method,

Figure 3 shows the transmission of a Zr filter foil on a mesh support grid of 60 µm wires. Figure 4 gives one line of data from Figure 3 (along red dashes) and Figure 5 zooms into this data with one nominal width of a wire (60 µm) indicated.

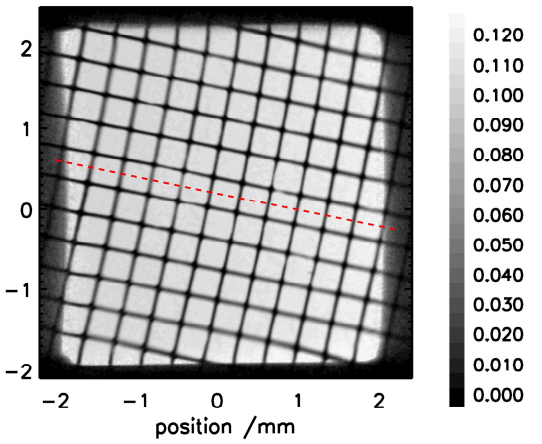

Figure 3:
Transmission of Zr-filter foil on support grid. Field on sample: 4 x 4 mm².
The scale gives transmittance values.

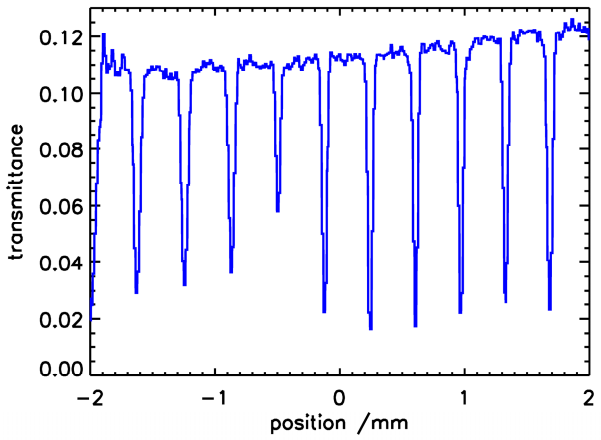

Figure 4:
Data from Figure 3 (along red dashes) showing varying width in the appearance of the gridlines due to aberration from the single toroidal mirror.

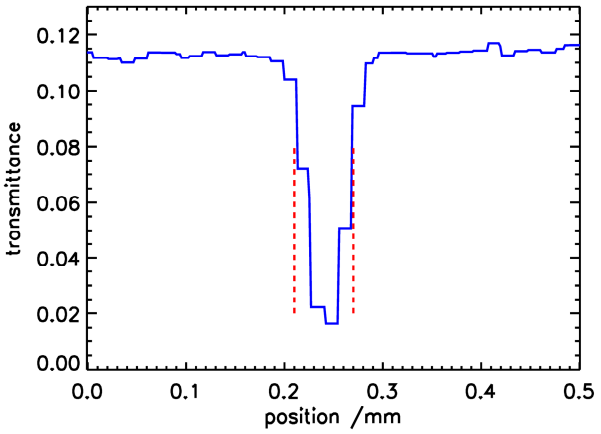

Figure 5:
Zoom into data from Figure 4 at best focus.
In red dashes, 60 µm are indicated
– the nominal width of a wire.

This imaging method of transmittance measurement can provide 2D transmission information much quicker than a mapping with a small beam. However, aberrations from the single toroidal mirror are noticeable outside the central field, being clearly visible in the curvature of the - straight - gridlines over the field.

2.2 Lubrication free measurement instrumentation at the Soft X-ray beamline

At the soft X-ray beamline, our instrumentation is lubrication free to prevent contamination on the samples during measurement. The instrument provides the freedom of movement to align a mask sized sample with the plane of reflection rotatable from horizontal (P-polarization) to vertical (S-polarization) [14].

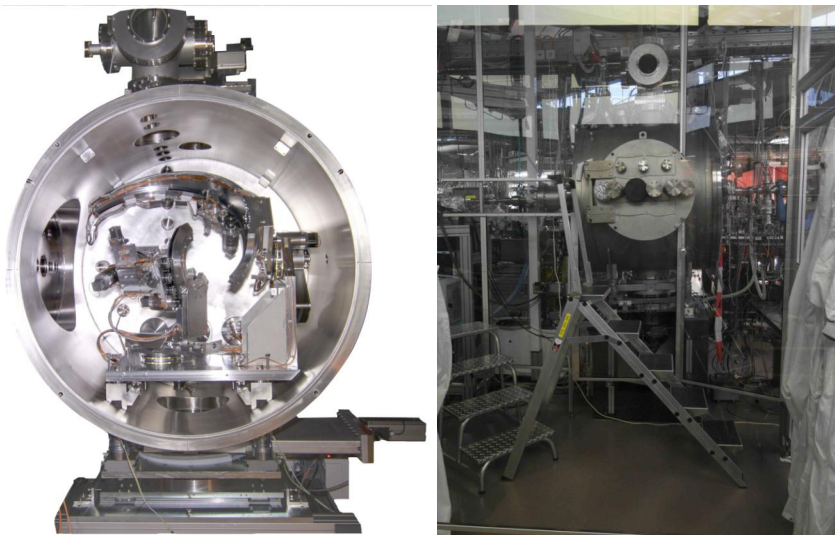

Figure 6: EUV Ellipso-Scatterometer of PTB. The sample stage can carry samples up to 190 mm square and 5 kg in mass. The mechanics are completely UHV compatible and lubrication free – left side. On the right side the instrument is shown in its cleanroom enclosure. The loadlock is visible on top, facing the viewer is the main access port.

With the loadlock opening into the recently installed cleanroom, optimal sample handling is possible. Figure 6 on the left side shows the goniometer inside its vacuum vessel. On the right side, the instrument is shown in its cleanroom enclosure - all sample handling can be performed under cleanroom conditions.

2.3 Exposure beamline

For lifetime tests, PTB operates a beamline which focuses radiation of a bending magnet into an exposure setup – see Figure 7. An elliptical rhodium coated mirror deflects the beam 20° and generates a focus. Out of the focus position, the beamspot becomes wedge shaped. The wedge shaped beam away from the focus together with the aperture blades available allow exposures using the higher flux small side of the wedge ('hot' spot), the lower flux wide side of the wedge ('cold' spot) or the full spot to expose both flux levels in one exposure. A Si/Zr filter is available for the exposure beam to suppress short wavelengths between 5 nm (the cut-off wavelength of the mirror) and 12.4 nm (the L absorption edge of Si) as well as long-wavelength VUV radiation by the Zr coating. In the 'hot' spot 20 W/cm^2 are available, using the 'cold' spot region of the beam as well as longer distance to the focus and further attenuation filters, the power density can be reduced in a reproducible and quantitative manner to a few mW/cm².

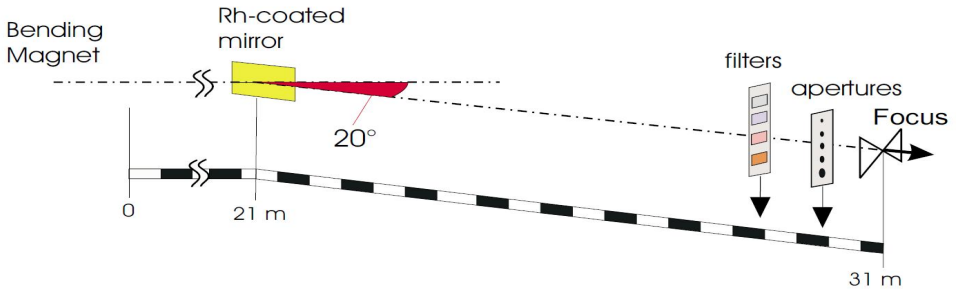

Figure 7: Scheme of PTB exposure beamline. Bending magnet radiation from BESSY II is focused into the experiment by a rhodium coated elliptical mirror under 20° deflection. The radiation can additionally be filtered and apertures are available to define the final spot on the sample.

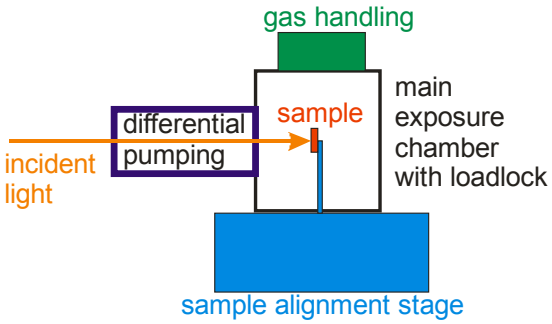

Figure 8:
The exposure setup is completely lubricant free and has 4 degrees of freedom to align the sample to the beam and – thanks to a differential pumping stage - allows to introduce a defined atmosphere. In the sample chamber, a pressure of 3 Pa can be maintained during exposure.

The exposure setup contains a sample stage with all drives outside the vacuum. It offers 3 linear degrees of freedom to align the sample to the beam and one rotational axis to adjust the angle of incidence as necessary. A differential pumping stage is integrated between the sample chamber and the beamline and allows keeping the sample in a defined atmosphere. In the sample chamber, a pressure of 3 Pa can be maintained during exposure. Figure 8 shows a block diagram of the exposure setup.

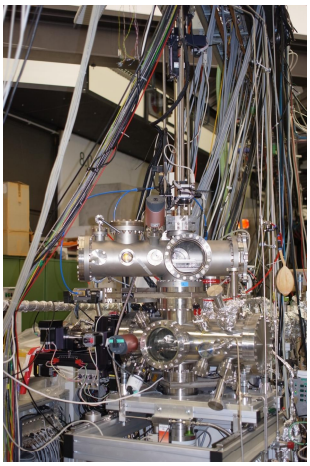

Figure 9:
Irradiation chamber with load-lock on top. On the right, needle valves for gas supply and on the left (in black) a 4-axis manipulator for positioning the samples. The load-lock system is designed for loading and unloading 1"-size GO substrates. There is the option for H*-cleaning in the loadlock chamber. The whole system can be moved on rails at the top of the rack to go to different focal distances (adjusting beam size and power density).

Samples are transferred into the exposure chamber via a loadlock which also offers the possibility of H* cleaning. Individual sample holders for 1" GO sized samples are available. Figure 9 shows the exposure setup and loadlock.

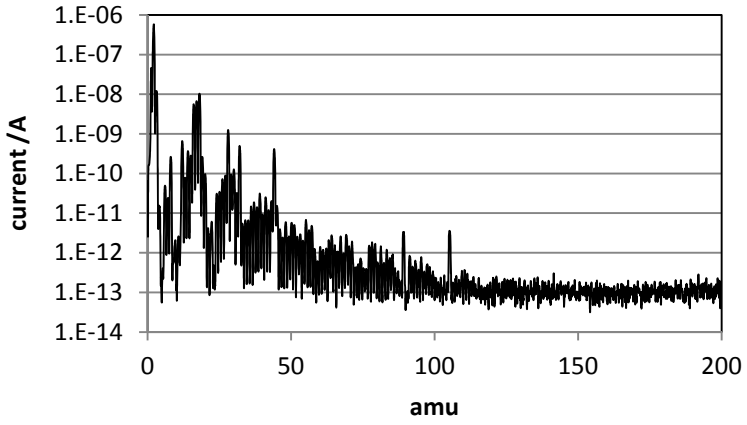

Figure 10:
After conditioning,
the base pressure of the exposure chamber is below $5 \cdot 10^{-7}$ Pa.
The RGA spectrum shown is an example.

Before exposures, the chamber is baked and pumped as necessary. A base pressure of below $5 \cdot 10^{-7}$ Pa has been achieved. Figure 10 shows an RGA spectrum of the exposure chamber.

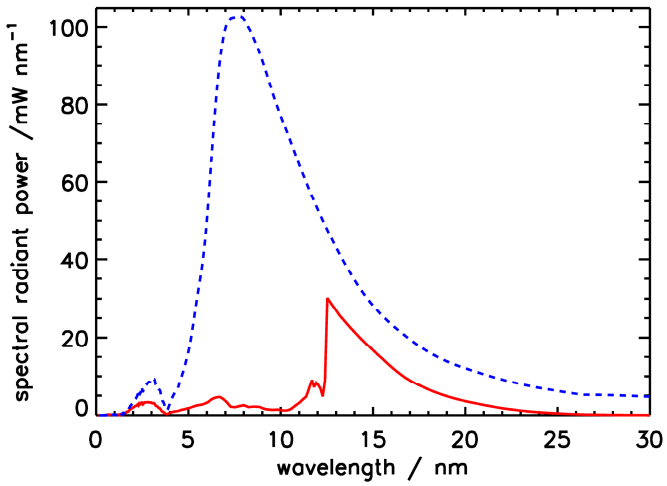

Figure 11:
Spectral distribution of the exposure radiation.
Spectrum of the synchrotron radiation after the grazing incidence mirror in blue dashes.
Cut off wavelength is 5 nm.
Spectrum of the radiation with a Si/Zr foil filter in the beam path in red, indicating a cut off wavelength of 12.4 nm at the Si-L absorption edge and a suppression of radiation beyond 25 nm.

The spectral distribution of the exposure radiation is shown in Figure 11. The white light from the bending magnet is cut off to shorter wavelengths at about 5 nm by the 10° angle of incidence reflection off the elliptical rhodium coated focusing mirror (blue dashes). An optional Si/Zr foil filter in the beam path cuts off radiation below 12.4 nm wavelength (Si-L absorption edge) and suppresses radiation beyond 25 nm (red line). To achieve a spectral distribution of EUV lithography bandwidth, the beam can be bounced off a multilayer mirror using a special sample mounting.

How the spatial distribution of power density is affected by focus distance can be seen in Figure 12 and Figure 13. Both distributions show the status with the Si/Zr filter in the beam path. 'Hot' and 'cold' part of the spot are clearly discernible.

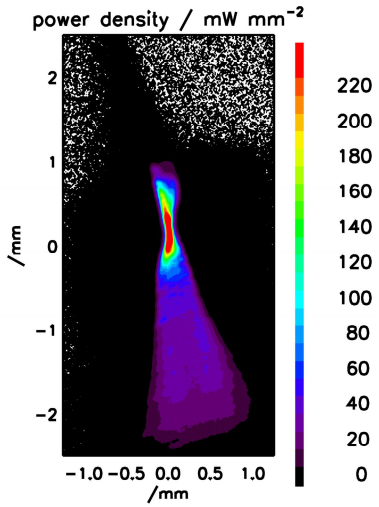

Figure 12: Spatial distribution of radiation at 161 mm distance from focus. Spectrum with Si/Zr filter in the beam path.

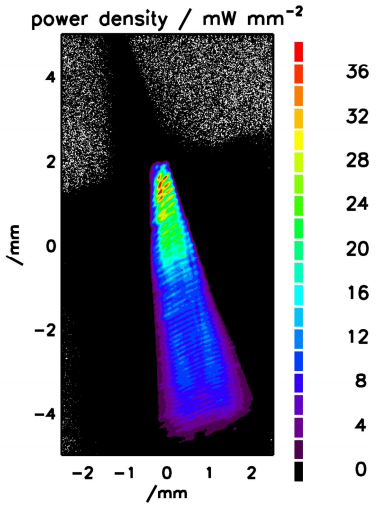

Figure 13: Spatial distribution of radiation at 334 mm distance from focus. Spectrum with Si/Zr filter in the beam path.

Radiant power on the sample can be chosen by selecting the appropriate part of the beamspot and adjusting distance from the focus. Figure 14 gives radiant power values for hot and cold spot over focus distance, the values apply with the Si/Zr filter in the beam path.

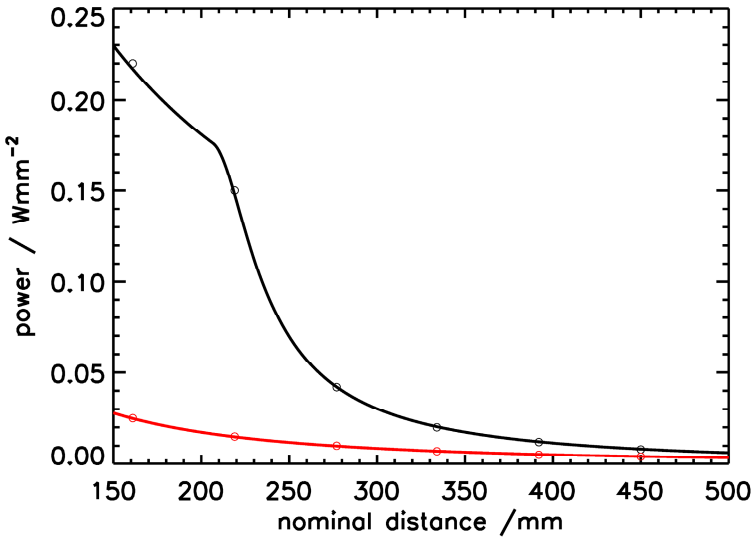

Figure 14:
Radiant power density available
with Si/Zr filter in the beam
at different distances from sample to focus.
In black: Radiant power density in hot spot
In red: Radiant power density in cold spot.

Figure 14 gives radiant power density in the beam over distance from focus. Black curve for the hot spot part of the beam, red curve for the cold spot part. Spot sizes and spatial radiant power distribution for two focus distances can be seen in Figure 12 and Figure 13.

3. CONCLUSIONS

To support materials development for EUV applications, PTB has extended and improved its instrumentation and methods with a focus on clean sample environment, improved spatial resolution transmittance measurements and EUV exposure studies. PTB now has available experience and a suite of instruments to perform radiometric characterizations such as transmittance and reflectance including polarization sensitivity [14] as well as scatterometry. The wavelength range available reaches from below 1 nm to 45 nm and beyond using spot sizes from 0.1 mm x 0.1 mm up to 4 mm x 4 mm. The PTB exposure setup provides radiant power density as high as 20 W/cm^2 for Si/Zr-filtered radiation. Apertures are available to cut the exposure beam spot if 'hot' spot or 'cold' spot only exposures are desired or as required geometrically. The sample to be exposed can be aligned in 4 axes. To match the available spectrum to EUV lithography requirements, a filter can be introduced. A defined atmosphere of up to 3 Pa can be maintained during exposure. Together, reflectometry and exposure capability available in the PTB synchrotron radiation lab provide a full set of tools to determine material properties and validate performance for EUV applications.

References

1 B. Beckhoff, A. Gottwald, R. Klein, M. Krumrey, R. Müller, M. Richter, F. Scholze, R. Thornagel, G. Ulm, "A quarter-century of metrology using synchrotron radiation by PTB in Berlin", Phys Status Solidii B, **246** 1415-1434 (2009)

2 R. Klein, C. Laubis, R. Müller, F. Scholze, G. Ulm, "The EUV metrology program of PTB", Microelectr. Eng. **83**, 707-709 (2006)

3 C. Laubis, A. Barboutis, M. Biel, C. Buchholz, B. Dubrau, A. Fischer, A. Hesse, J. Puls, C. Stadelhoff, V. Soltwisch, F. Scholze, "Status of EUV Reflectometry at PTB", Proc. SPIE **8679**, 867921 (2013)

4 F. Scholze, J. Tümmler, G. Ulm, "High-accuracy radiometry in the EUV range at the PTB soft X-ray radiometry beamline", Metrologia **40**, S224-S228 (2003)

5 F. Scholze, et al., "High-Accuracy EUV Metrology of PTB Using Synchrotron Radiation", Proc. SPIE **4344**, 402–413 (2001)

6 C. Laubis, F. Scholze, G. Ulm, "Metrology in the Soft X-Ray Range – from EUV to the Water Window", Proc. SPIE **7101**, 71011U (2008)

7 B. Mertens, B. Wolschrijn, R. Jansen, N. Koster, M. Weiss. M. Wedowski, R. Klein, T. Bock, R. Thornagel, "EUV time resolved studies on carbon growth and cleaning", Proc. SPIE **5037**, 95-102 (2003)

8 C. Laubis, A. Fischer, F. Scholze, "Extension of PTB's EUV metrology facilities", Proc. SPIE **8322**, 832236 (2012)

9 R. Klein, R. Thornagel, G. Ulm, J. Feikes, G. Wüstefeld, "Status of the Metrology Light Source", J. Electron Spectrosc. **184** (2011) 331-334

10 C. Laubis, F. Scholze, C. Buchholz, A. Fischer, S. Hesse, A. Kampe, J. Puls, C. Stadelhoff and G. Ulm, " High accuracy EUV reflectometry at large optical components and oblique incidence", Proc. SPIE **7271**, 72713Y-1 (2009)

11 F. Scholze, A. Kato, C. Laubis, "Characterization of nano-structured surfaces by EUV scatterometry", J. Phys, Conf. Ser. **311**, 012006 (2011)

12 F. Scholze, R. Klein, R. Müller, "Characterization of detectors for extreme UV radiation", Metrologia **43**, S6-S10 (2006)

13 L. Shi, S. Nihtianov, F. Scholze, A. Gottwald, L. Nanver, "High-sensitivity high-stability silicon photodiodes for DUV, VUV and EUV spectral ranges", Proc. SPIE **8145**, 81450N (2011)

14 V. Soltwisch, A. Fischer, C. Laubis, C. Stadelhoff, F. Scholze, A. Ullrich, "Polarization resolved measurements with the new EUV Ellipsometer of PTB", Proc. SPIE **9422**, 942213 (2015)